Computers, Materials & Continua

Tech Science Press

DOI: 10.32604/cmc.2024.057991

ARTICLE

Research on Multimodal Brain Tumor Segmentation Algorithm Based on Feature Decoupling and Information Bottleneck Theory

Xuemei Yang[1], Yuting Zhou[2], Shiqi Liu[1] and Junping Yin[2,3,*]

[1]China Academy of Engineering Physics, Graduate School, Beijing, 100193, China

[2]Shanghai Zhangjiang Institute of Mathematics, Biomedical Laboratory, Shanghai, 201203, China

[3]Institute of Applied Physics and Computational Mathematics, Tang Chuang Centre, Beijing, 100094, China

*Corresponding Author: Junping Yin. Email: yin_junping@iapcm.ac.cn

Received: 02 September 2024 Accepted: 06 December 2024 Published: 17 February 2025

ABSTRACT

Aiming at the problems of information loss and the relationship between features and target tasks in multimodal medical image segmentation, a multimodal medical image segmentation algorithm based on feature decoupling and information bottleneck theory is proposed in this paper. Based on the reversible network, the bottom-up learning method for different modal information is constructed, which enhances the features' expression ability and the network's learning ability. The feature fusion module is designed to balance multi-directional information flow. To retain the information relevant to the target task to the maximum extent and suppress the information irrelevant to the target task, the feature decoupling module is designed to ensure a strong correlation between the feature and the target task. A loss function based on information bottleneck theory was intended to improve information quality and remove redundant information. Based on BraTs2021, BraTs2023-MET and ANNLIB datasets, the proposed algorithm is analyzed qualitatively and quantitatively in this paper. In the quantitative experiment, the Dice coefficient of the proposed algorithm was increased by 0.110 on average compared with other methods, and the HD95 was decreased by 28.568 on average compared with other methods. In qualitative analysis, the proposed algorithm can effectively segment the incoherent region between the lesion and the lesion boundary and achieve accurate segmentation of the lesion.

KEYWORDS

Image fusion; image segmentation; deep learning

1 Introduction

In recent years, with the development of artificial intelligence algorithms, data-driven algorithms are constantly changing from single-modal data to multimodal data. The theories and methods in mathematics and information provide theoretical support for studying the mechanism of multimodal data fusion and mining the potential information association of cross-modal data. Multimodal medical image data analysis aims to improve the expression ability of features by fusing the input data of different modalities according to a specific mechanism to identify the lesion area or stage the lesion accurately. Among them, explaining the principle of multimodal medical image segmentation

and building the algorithm through information change is a crucial task of multimodal medical image analysis.

Medical image segmentation is mainly used to extract the contour of interest from medical imaging data. This process performs pixel-wise partitioning by identifying anatomical structures in the image. Multimodal magnetic resonance imaging (MMRI) medical images can help doctors fully grasp the specific characteristics of anatomical information of different brain lesions and improve the segmentation performance. In the segmentation task of abnormal brain lesions, the location distribution, pixel intensity distribution, and lesion shape vary significantly among different samples, which causes problems with the multimodal segmentation task, such as information loss and inaccurate segmentation results. There is redundant information between medical images of different modalities, which will cause the joint learning algorithm to misjudge the importance of different modalities [1], ignore specific modality information and eventually reduce the prediction accuracy and lead to overfitting [2]. Therefore, this paper studies multimodal brain tumor image segmentation methods based on MMRI data. Currently, the standard image segmentation methods based on deep learning, such as the model based on Fully Convolutional Networks for semantic segmentation (FCN), the model based on U-Net, and the model based on Transformer, have gradually become the mainstream methods for multimodal brain tumor image segmentation. The core of these methods is to map the original data into a higher-dimensional feature space through complex, multi-dimensional, nonlinear array operations and to abstract the data into features that are more satisfying for downstream tasks through segmentation network training. The proof of Radmacher's complexity shows that the quality of feature space directly affects the accuracy and generalization of the model. We expect to construct a feature space as complete as possible through the design of the network structure to maximize the contribution of the feature space to the task. The feature space will provide the information associated with the given task, suppress the information that interferes with the task, and complete a task-oriented data "compression" work to avoid information redundancy and information loss caused by the design of the network structure. However, these segmentation networks cannot accurately classify at the pixel level because the size of the feature map will gradually decrease during the downsampling process, which affects the effect of precise segmentation. For example, the FCN model replaces the convolutional layer with the deconvolution layer to achieve upsampling. However, the deconvolution layer lacks the mechanism of parameter sharing, leading to its failure to capture the global features in the image, thus losing part of the semantic information. The U-Net model captures image features by multiple down-samplings in the encoder, but when the original size of the image is restored by various up-samplings in the decoder, some details and semantic features will be lost, making the segmentation results inaccurate enough. The Transformer model only considers single-scale feature representation, which will cause information loss.

Aiming at the problems of existing medical image segmentation algorithms, this paper proposes a brain tumor MMRI segmentation network based on feature decoupling and information bottleneck theory: FDIBMNet. The main contributions are as follows:

(1) Based on the reversible network, a multi-direction flow and multi-branch encoder with bottom-up and multimodal information interaction is constructed, which allows information to flow across layers among branches, realizes the transfer of low-level detailed information and high-level semantic information between modes, enhances the expression ability of features and the learning ability of the network and helps the network to maintain richer and more comprehensive information and avoid information loss.

(2) To maintain the information balance of multi-directional flow, the feature fusion module is designed, and the interdependence between feature channels is established to realize the adequate flow and fusion of features between different resolutions, maintain their information is not compressed or lost, and form a feature representation without information loss.

(3) Construct a feature space as complete as possible, maximize its contribution and correlation information to the task, and suppress information that has no contribution and correlation to or interferes with the task. Firstly, based on the topological properties of medical images (pixel connectivity and adjacency), a feature decoupling module is designed to decouple the relationship between pixels and geometric properties of medical image features from the feature space and to model and enhance the topological representation between interested pixels. Secondly, based on the information bottleneck theory, loss constraints were applied to multimodal features to ensure a strong correlation between features and tasks and remove redundancy, and third, based on the mutual information constraint between input and output, decoupling the sharing and uniqueness of multimodal features.

This paper is organized as follows: Section 2 introduces related work. Section 3 introduces the network structure of the algorithm constructed in this paper in detail. Section 4 conducts detailed experiments and evaluates the experimental results. Section 5 summarizes the findings, contributions, and limitations of this paper.

2 Related Works

The medical image segmentation method based on deep learning, combined with the basic principles of computer vision, can realize the automatic recognition and segmentation of the foreground area of the lesion area and the background area, such as organs and tissues, through the fine pixel classification of the medical image, without the need for manual feature design and extraction. Through convolution and pooling operations, finer high-level semantic features are gradually extracted, making the segmentation results closer to the actual situation. Deep learning technology improves the accuracy and segmentation efficiency of medical image analysis and supports the early detection, diagnosis, and treatment of diseases. Standard supervised learning segmentation algorithms include medical image segmentation algorithms based on the FCN framework, medical image segmentation algorithms based on the U-Net framework, and medical image segmentation algorithms based on Transformer framework.

FCN is a classical image segmentation method. By converting the Convolutional Neural Network (CNN) structure into a fully convolutional structure, the network can output a segmentation result the same size as the input image. FCN utilizes convolutional and deconvolution operations to learn the category label of each pixel in the image to achieve pixel-level segmentation. Sun et al. [3] proposed multi-channel FCN for liver tumor segmentation from CT images. Each stage of contrast-enhanced CT images provides different information about pathological features, so a network is trained for each stage of contrast-enhanced CT images, and their high-level features are fused to achieve automatic liver tumor segmentation of CT images. Ben-Cohen et al. [4] proposed an algorithm for segmenting liver cancer metastases on CT, combining FCN with super-pixel sparse classification to achieve accurate segmentation of small lesions and reduce the false positive rate. Feng et al. [5] proposed a multi-stage FCN architecture for 2D MRI segmentation of the prostate. The algorithm can capture more accurate spatial information and prostate boundaries through different sequences of MRI. Compared with CNN-based image segmentation methods, FCN can accept input images of any size and become more efficient without size transformation. However, FCN does not fully consider the relationship

between pixels, and the pixel-level segmentation results still cannot meet the requirements of accurate segmentation. The medical image segmentation method based on the U-Net framework can deal with the above problems of FCN well.

Unlike the segmentation task of natural scene images, medical images usually contain artifacts, and the boundary of the region of interest is blurred and unclear. U-Net can effectively combine low-resolution features with high-resolution features through jump connections, and it has become a benchmark framework for most medical image segmentation tasks. Chen et al. [6] proposed a long-range sensing model for the segmentation of fuzzy boundaries of medical images, which has long-range solid sensing ability and can effectively perceive the semantic context information of the entire image. Experimental results show that the proposed algorithm is more effective in improving the segmentation accuracy of fuzzy boundary regions than other long-distance sensing methods such as Transformer. Yu et al. [7] proposed a differential evolution algorithm based on U-Net for medical image segmentation. The algorithm relies on the expertise of differential evolution to search neural networks automatically. The variable length encoding strategy is used to optimize the neural architecture, effectively improving brain tumors' segmentation effect. Zhang et al. [8] proposed an algorithm integrating densely connected convolutional modules into the U-Net architecture. By replacing the standard convolutional layer with dense connections, the width of the network is increased, and the features are extracted without increasing the parameters to make the network deeper. In the research of multimodal fusion data analysis algorithms for brain tumors, a downsampling block is used to reduce the size of the feature map to accelerate learning, and an upsampling block is used to adjust the size of the feature map to achieve accurate reconstruction of segmented images. The algorithm achieves precise segmentation of brain tumors on MRI.

U-Net algorithm can obtain high-precision segmentation results in image segmentation tasks of various modalities and diseases, especially when dealing with small targets or images with complex details. U-Net network architecture is relatively simple, easy to implement, and understand. However, the encoder part of U-Net mainly focuses on extracting local information, and it is challenging to integrate global information, which may lead to poor performance in processing long-distance dependency and context information, especially in the task of medical image segmentation. At the same time, during the coding process of U-Net, the down-sampling operation will lose part of the spatial information, which is a challenge for tasks that require accurate spatial localization. The decoder part of U-Net makes it difficult to effectively recover global information during upsampling, which may lead to decreased accuracy of segmentation results. Compared with U-Net, the medical image segmentation algorithm based on the Transformer framework can deal with global information well.

The medical image segmentation algorithm based on the Transformer framework captures the long-distance dependence through the self-attention mechanism and effectively processes the global information in the image. Jiang et al. [9] proposed a label decoupling network with a space-channel graph convolution and a dual attention enhancement mechanism. The algorithm constructs learnable adjacency matrices and uses graph convolution to efficiently capture global long-range information on spatial locations and topological dependencies between different channels in an image. The dual attention enhancement mechanism is constructed, and the edge attention mechanism module is designed in the edge branch to promote the learning ability of spatial region and boundary features. The algorithm can retain the spatial location information in the medical image and improve the accuracy of medical image segmentation. Zhang et al. [10] used spatial pyramid pooling instead of pooling layers as encoders and integrated attention mechanisms to capture complex cross-dimensional interaction information. Extensive experimental results on brain tumor segmentation datasets show that the proposed algorithm performs excellently in medical image segmentation. Li et al. [11] proposed

a mutually reinforcing multi-view information model for lung tumor segmentation. The model uses the attention mechanism to enhance node attributes, designs the gated convolution strategy to integrate the enhanced attributes and original features, constructs the learning context of the multi-channel CT, and realizes cross-channel information fusion. Multi-view mutual information is fused through an interactive attention mechanism. Finally, the node embedding, channel context embedding, and original features are adaptively integrated, and the final output is obtained through the segmentation decoder.

Medical image segmentation algorithms based on the Transformer framework can better model the global context to understand the information in complex medical images. The framework is easy to extend and can further improve the effect of medical image segmentation by increasing the number of layers, input images of different sizes, and adjusting the model size. However, Transformer can only consider global information and has a weak ability to extract cross-domain information.

In conclusion, the medical image segmentation method based on the deep learning framework is superior to the traditional medical image segmentation method, but there are still the following problems:

(1) The direction of segmentation will be limited when the algorithm based on the deep learning framework is used for medical image segmentation. For MRI image segmentation with complex boundaries, such as brain tumors, we can modify the direction of segmentation by adjusting the form of the loss function further to improve the accuracy of brain tumor image segmentation.

(2) The core of the neural network is to map the input data into the feature space through complex, multi-dimensional, and nonlinear array operations and perform feature transformation and nonlinear transformation layer by layer. The original data is mapped into a higher dimensional feature space as the hierarchy is gradually deepened. In this feature space, the data is abstracted into semantic features that are more satisfying for the downstream task. The construction of feature space is closely related to the accuracy and generalization ability of the model. This study expects to map data from the original data space to the "representation space" through network design. Through the training of neural networks, it is expected to maximize the information that contributes to the task and is related to the task and suppress the information that does not contribute to the task, is not associated with the task, or has interference with the task. Perform a kind of data "compression" for downstream tasks.

(3) During the construction of neural networks, avoiding the loss of information caused by the design of network structure is necessary. For example, in the shared segmentation network downsampling process, the size of the feature map will gradually decrease, which cannot represent the specific contour of the object and cannot classify the organization of each pixel, so the goal of accurate segmentation cannot be achieved. However, downsampling can reduce the computational complexity of deep networks and is widely used in network structure design. Therefore, it is necessary to balance feature extraction and computational complexity.

3 Methodology

Clinically common MRIs usually contain a variety of different sequences, and different sequences are used to examine different anatomical structures, Common sequences include T1-Weighted Imaging (T1WI), T1-weighted Gadolinium enhanced Imaging (T1Gd), T2-Weighted Imaging (T2WI), and Fluid Attenuated Inversion Recovery (FLAIR). The T1WI sequence showed clear anatomical structure and bleeding, and brighter adipose tissue, with relatively few artifacts, but the lesion was not clearly displayed. The contrast between blood vessels and brain tissue is more obvious in T1Gd

sequence, so the blood vessels and lesions of the brain can be more clearly displayed. T2WI sequence is contrary to T1WI sequence, which is clearer for lesions and edema, especially for the diagnosis of brain tumors. The FLAIR sequence can be used to determine the edema area around the tumor. Although MRI takes a long time to image, it is widely used for accurate screening of diseases in clinic because it has no radiation and can observe different anatomical structures and tissue information through different sequences.

Fig. 1 shows the design of the feature decoupling and information bottleneck theory image segmentation network (FDIBMNet) framework. The model consists of an encoder, a feature decoupler, and a decoder. In the encoder part, X_1, X_2, X_3, X_4 correspond to the four modes of MMRI (T1WI, T1Gd, T2WI, and FLAIR). Taking X_1 as an example, the output information of Level1 of X_1 will be passed to the output of Level1 of X_2 and fused with the output of Level1 of X_2, which will be used as the input of Level2 of X_2 for subsequent processing. At the same time, the output information of Level2 of X_1 will flow to the input of Level1 of X_2 and be fused with the input of X_2, which will be used as the input of Level1 of X_2 for subsequent processing. After the four modes X_1, X_2, X_3, X_4 all adopt bottom-up and information interaction between modes, the encoder is completed.

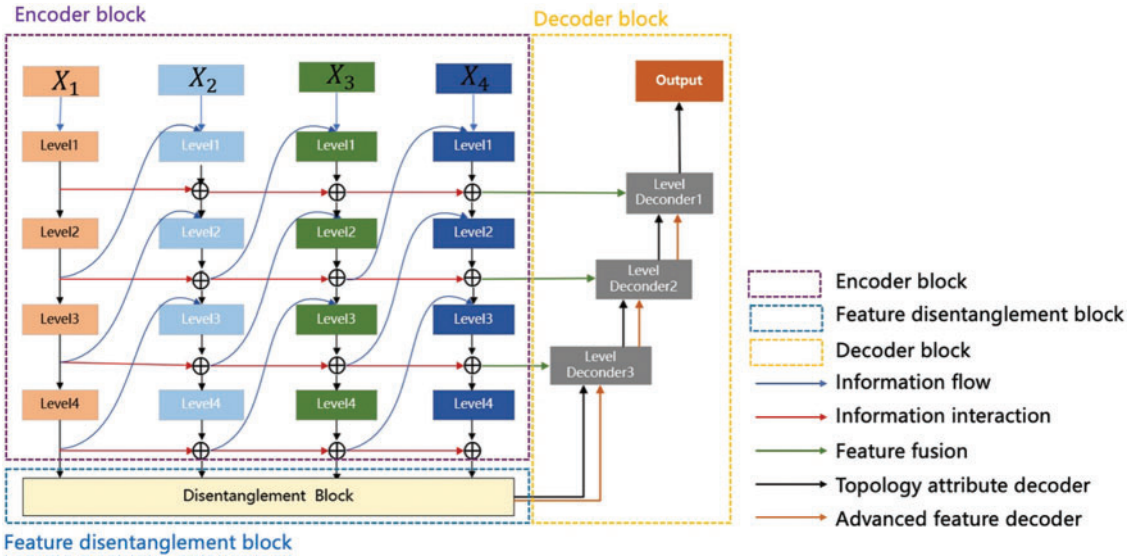

Figure 1: FDIBMNet's framework

The information between different modalities may have shared or unique information related to the target task, and the information between modalities may have similarities or differences. Only by fully characterizing the information of the modalities can the results of the target task be maximized. Through the interaction of information, the encoder fully represents the modal information and ensures a strong correlation between the information in the feature and the target task. The basic design principle of the feature decoupler comes from the region-growing algorithm. Firstly, the pixel value of the center of the lesion will be given, and the relationship between the surrounding pixels and the pixels of the lesion will further expand the segmented area. When the surrounding pixels are unrelated to the pixels of the lesion area, the boundary delineation of the lesion will be completed. The feature decoupler is set up based on this idea. Through feature coupling and combined with the decoupling directional features, the feature decoupling device ensures the consistency of the anatomical position in the image and completes the extraction of semantic information related to the lesion boundary. In

the decoder part, high-level features, topological attributes, and information fusion are used to decode the extracted semantic information and topological characteristics in parallel, which ensures that the structure shape, pixel brightness, texture features, and the relationship between the representation pixel and the surrounding neighborhood are preserved at the same time in the decoding process, and the lesion segmentation is effectively realized.

3.1 Encoder Structure

The encoder comprises four parallel branch encoders containing different levels of feature extraction blocks, and the transmission of lossless information is maintained by a multi-level reversible connection between two adjacent columns. In forward propagation, this architecture scheme can ensure that the information in the model flows in two ways: one is the "top-down" information transmission to achieve single-mode feature extraction, and one is "bottom-up" information transmission to achieve cross-modal and cross-level information interaction. Specifically, multimodal image data X_1, X_2, X_3, X_4 are input, and feature extraction is performed as shown in Fig. 1. The feature mapping process is divided into Level1, Level2, Level3, and Level4. Between each column, reversible joins are introduced to preserve the propagation of lossless information. The feature transfer process is mainly as follows:

$$F^l = F_{i,j} \oplus F_{i-1,j} \tag{1}$$

$$F_{i,j+1} = LE_{i,j+1}(F^l, F_{i-1,j} + 2) \tag{2}$$

$$F_{i,j} = LE_{i,j}(\cdot) \tag{3}$$

where, i represents the four modal numbers, $i = \{1, 2, 3, 4\}$ corresponding to X_1, X_2, X_3, X_4, j represents the four levels $j = \{1, 2, 3, 4\}$, corresponding to Level1, Level2, Level3, Level4. $F_{i,j}$ represents the feature extracted from the input information (feature information or source data) of the ith modality through the feature coding module of the jth level. $\oplus$ means adding the corresponding elements to the feature matrix. $LE_{i,j}$ represents the (Level encoder block, LB) coding module of the jth level under the ith modal branch, as shown in Fig. 2.

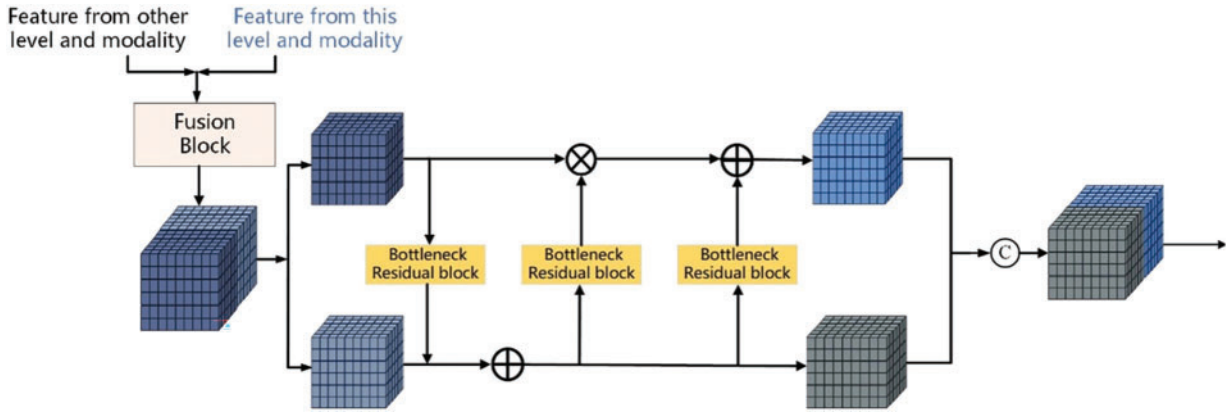

Figure 2: Encoder structure: Level encoder block

This parallel branch structure gradually decouples features during the forward propagation process to maintain the integrity of information and avoid information compression or loss. The

bidirectional flow of information between multiple branch networks is allowed so that in the process of forward propagation, each branch structure can receive the information of other branch structures and pass the processed results to the next layer of other branches while retaining all the information in the transmission process.

In forward information propagation, a CNN-based structure is constructed to realize the mapping of input data to features. Ideally, if the extracted features can be "reconstructed" from the input data through some backward process, the information is not lost and is effective in the forward process. Combined with the background of multimodal medical image segmentation in this chapter, it is hoped to design a network structure to ensure the effective extraction and lossless transmission of information such as anatomical characteristics, structure shape, pixel brightness, texture features, and the relationship with surrounding tissues of abnormal brain lesions during the information transformation of input medical images. This is important for later brain lesion tissue segmentation tasks.

Invertible Neural Networks (INNs) is a particular type of neural network whose main feature is that the mapping from input to output is bidirectional and reversible. This property makes the backpropagation and gradient calculation of the network more efficient and reliable and can better achieve data reconstruction and reduction and maintain the integrity of information in the task. INNs are a lossless feature extraction architecture, which is very suitable for information retention and network training in multimodal image fusion. Based on INNs, this paper proposes constructing LB with INNs blocks with affine coupling layers to realize feature extraction and lossless transfer, as shown in Fig. 3a,b [12].

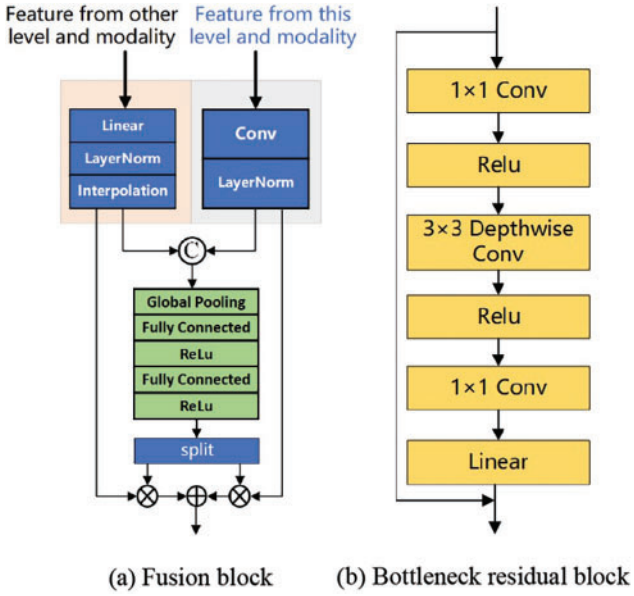

Figure 3: Encoder structure: Fusion block and bottleneck residual block

Firstly, the feature map $F_l^{X_i}$ from mode X_i and network layer $Level_{l-2}$ is fused with the feature map $F_{l-2}^{X_j}$ from mode X_j and network layer $Level_{l-2}$. The feature maps of different resolutions are unified to the same size ($h \times w \times c$) by upsampling and downsampling operations and stacked along the channel dimension to obtain the feature $F \in \mathbb{R}^{h \times w \times 2c}$. Through the combination of global pooling, full connection and activation function, the stacked feature $F \in \mathbb{R}^{h \times w \times 2c}$ is compressed and the channel is

excited, and the importance degree of $2C$ channels is learned to obtain the weight $W \in \mathbb{R}^{1\times1\times2c}$. Then $F \in \mathbb{R}^{h\times w\times2c}$ and $W \in \mathbb{R}^{1\times1\times2c}$ sequence division (split) for specific characteristics to two groups of the same number of channels $F_c \in \mathbb{R}^{h\times w\times c}$ and $F_{C'} \in \mathbb{R}^{h\times w\times c}$ and weight $W \in \mathbb{R}^{1\times1\times c}$ and $W_{C'} \in \mathbb{R}^{1\times1\times c}$ and weighted as follows:

$$F_{fusion} = (F_c \otimes W_c) \oplus (F_{C'} \otimes W_{C'}) \tag{4}$$

where, F_c and $F_{C'}$ denote the features of the same number of channels obtained by sequential splitting, and W_c and $W_{C'}$ are the weights of F_c and $F_{C'}$. $\oplus$ indicates the addition of the corresponding elements in the eigenmatrix and $\otimes$ indicates the multiplication of the corresponding elements in the eigenmatrix. In this process, the interdependence between the feature channels is explicitly modeled, and the feature map $F_l^{X_i}$ from the mode X_i and the network layer $Level_l$ is projected into the feature space where the feature map $F_{l-2}^{X_j}$ of the mode X_j and the network layer $Level_{l-2}$ is located. To achieve effective flow fusion of features between different resolutions and modes, maintain their information without compression or abandonment, and generate a new feature representation F_{fusion}.

The information Bottleneck Residual block (BR) takes the low-dimensional compressed representation as input, first extends it to higher dimensions, and then convolutional layers are used for convolution. Features are subsequently projected back to a low-dimensional representation with linear convolutions. The lossless feature F_{INNs} is obtained by taking F_{fusion} as input to INNs with affine coupling layers. As shown in Fig. 3, F_{fusion} is divided into two parts from the channel dimension, denoted as $F^F_{[1:c]}$ (1 to c channels) and $F^F_{[c:C]}$ ($c+1$ to C channels).

$$F^1_{[c+1:C]} = F^F_{[c+1:C]} \oplus \mathrm{BR}(F^F_{[1:c]}) \tag{5}$$

$$F^1_{[1:c]} = F^F_{[1:c]} \otimes BR(F^1_{[c+1:C]}) \tag{6}$$

$$F^2_{[1:c]} = BR(F^1_{[c+1:C]}) \oplus F^1_{[1:c]} \tag{7}$$

$$F_{INNs} = Concat(F^2_{[1:c]}, F^1_{[c+1:C]}) \tag{8}$$

where, *Concat* represents the feature stack, $F^F_{[1:c]}$ represents the 1 to c channel features of F_{fusion}, $F^F_{[c+1:C]}$ represents the $c+1$ to C channel features of F_{fusion}, The new feature $F^1_{[c+1:C]}$ of the $c+1$ to C channels is obtained by adding BR and corresponding elements. $F^1_{[c+1:C]}$ and $F^F_{[1:c]}$ after BR and the corresponding elements multiplication get to c channel new features $F^F_{[1:c]}$. $F^1_{[1:c]}$ and $F^1_{[c+1:C]}$ get one after BR and corresponding element addition to c channel new features $F^2_{[1:c]}$. $F^2_{[1:c]}$ and $F^1_{[c+1:C]}$ after feature stacking give lossless features F_{INNs}.

According to the properties and characteristics of the reversible network, the connection of two side branches can be set to any mapping without affecting the lossless information transmission in this reversible layer. Considering the trade-off between computational consumption and feature extraction power, we adopt BR in MobileNetV2 as the connection of two side branches in the INNs structure. As shown in Fig. 3b, after the features enter the BR, the dimension of the input feature map is increased by 1×1 convolution, the number of channels is increased, and the mainstream information is stored in the subspace of the high-dimensional space, which provides the basis for the reversibility of the model. Subsequently, all channels were aggregated by 3×3 Depth wise separable convolution (DSC), and the spatial features and channel features were extracted from the information after dimension upgrading. DSC mainly performs group convolution on the feature dimension, first performing an independent depth-by-depth convolution operation on each channel and then performing a 1×1 point-by-point convolution operation on all channels. In this process, the number of channels remains unchanged,

but the length and width of the feature map become smaller, thereby reducing the parameters required by the convolutional layer and improving the computational efficiency. At the end of BR, the original number of channels is restored by 1×1 convolution. This process of first dimension upgrading, DSC convolution processing, and then dimension reduction allows the expressiveness of input and output domains to be decoupled from feature extraction, improves the performance of the model, reduces redundant information, and ensures that the information transmitted through the network can better serve the segmentation task.

Based on INNs, a multi-direction flows multi-branch encoder with bottom-up and inter-modal information interaction is constructed. This design avoids the common information loss problem in traditional deep networks, especially when the network level is profound. Therefore, this design can maintain rich feature representations in deep networks, improving the model's ability to represent data and learning efficiency. However, the output features of reversible networks mix the useful and useless information of the current task, and it is not easy to achieve a good feature expression ability. Therefore, features need not only to keep the information intact but also to decouple representations.

3.2 Feature Disentanglement

Feature disentanglement describes separating different features or factors in data representation. In some cases, the input data may contain multiple related but distinct features that may be intricately intertwined in complex ways. The goal of feature decoupling is to decompose these mixed features so that the model can learn the representation of each feature independently to extract more meaningful and practical information. The model can better understand the input data's intrinsic structure and hidden information with feature decoupling. Feature decoupling usually involves the specific design of the network structure, such as using regularization techniques or adding penalty terms in the loss function to encourage the independence of features. Through feature decoupling, the model is expected to learn more robust and distinguishable feature representations to perform better when facing unknown data. Feature decoupling is a strategy to ensure the quality of features.

Maintaining anatomical consistency in medical image segmentation is essential but extremely challenging, as even minor geometric errors may alter global topological properties and lead to functional errors in downstream clinical decisions. Anatomical consistency in an image can be represented by topological properties, such as pixel connectivity and adjacency [12]. Deep learning-based segmentation methods have made significant progress in capturing inter-pixel dependencies within the latent space of the network using encoder-decoder architectures. Currently, typical segmentation networks model the segmentation problem as a pixel-by-pixel classification task and use segmentation masks as unique labels. However, this pixel-by-pixel modeling scheme is suboptimal because it does not directly exploit inter-pixel relations and geometric properties. Therefore, these models may lead to low spatial coherence in the prediction, that is, inconsistent prediction of neighboring pixels with similar spatial features [13]. When applied to medical data with high noise and artifacts, low spatial consistency may lead to the problem of insufficient extraction of topological attributes. Pixel connectivity has long been used to ensure the fundamental topological duality of separation and connectivity in digital images [14]. For problem modeling, using connectivity masks essentially changes the problem from pixel-by-pixel classification to connectivity prediction, thereby modeling and enhancing the topological representation between pixels of interest. Compared with the segmentation mask, using the connectivity mask as the training label representation provides more information in the following three aspects: first, the connectivity mask stores the classification information between the connections of pixels and has the perception of the relationship between pixels; Second, edge pixels can be represented sparsely [15]; Third, it contains a wealth of directional connection information. Therefore, the latent

space constructed by the neural network trained with the connectivity mask has both pixel category features and directional features, and each feature exists in a specific subspace of the latent space. In previous studies [16], these two sets of features are learned simultaneously, maintaining a high coupling in the latent space and introducing redundancy [17]. However, the separation of meaningful subspaces from feature Spaces has been shown to effectively explain the dependence and independence between features. Inspired by feature space decoupling, this study considers decoupling subspaces with different feature meanings from feature space when performing feature extraction and uses the decoupling directional features to enhance the overall data representation for the convenience of subsequent analysis.

The features from the four modalities were first fused. The features $F = \{F_1, F_2, F_3, F_4\}$ from the four modes were stacked. Through the combination of global pooling, total connection, and activation function, the excitation weights $W = \{W_1, W_2, W_3, W_4\}$ of multiple channels in the full mode were obtained, which were added to the corresponding channel weights of feature F. The specific operation process is shown in the figure above and explained by Eqs. (9) to (12).

$$F_0 = Concat\,(F) = Concat\,(F_1, F_2, F_3, F_4) \tag{9}$$

$$F_1 = ReLu\,(Fully\ Connected\,(Global\ Pooling\,(F_0))) \tag{10}$$

$$W = Split\,(ReLu\,(Fully\ Connected\,(F_1))) \tag{11}$$

$$F_{fusion,2} = (F_1 \otimes W_1) \oplus (F_2 \otimes W_2) \oplus (F_3 \otimes W_3) \oplus (F_4 \otimes W_4) \tag{12}$$

where, F_0 represents the feature obtained by stacking four modal features, input to the global pooling, and fully connected layers. F_1 is obtained through the activation function, and then F_1 is input to the fully connected layer and the activation function for feature disassembly to obtain W. After element multiplication of the weights of different modes with the corresponding modes, $F_{fusion,2}$ was obtained by adding the elements of the results obtained from different modes. Since the network structure in this paper is designed for multi-directional flow, the input information of encoders at different levels and branches integrates the current and auxiliary modes' characteristics. This design can reduce the loss of different mode information, but it will also lead to the redundancy of features in different spatial states. Through the design of the fusion module here, the features learned by different modes and branches of encoders are uniformly mapped into the same feature space. Finally, the global spatial information is integrated by global pooling. The importance of $F = \{F_1, F_2, F_3, F_4\}$ is measured in the total modal feature space so that the international characteristics of spatial information are retained, and it is more robust to the spatial changes of the input image.

Due to the simultaneous connectivity between category features (whether they belong to a lesion tissue) and orientations in different pixels, it is natural to store orientation information between channels with the deepening of the network. Therefore, each channel of the fused multimodal feature map $F_{Fusion,2}$ is highly coupled with topological properties and class features. Based on this feature, we can decouple the orientation subspace from the shared latent space through a series of feature channel processing, and we can use the extracted orientation features to enhance the overall topological representation.

$F_{Fusion,2}$ is the final output feature of the encoder, which contains rich high-level semantic features, topological features, and low-discriminative pixel category features and shows the high correlation of pixel category features in the channel dimension. The purpose of dividing $F_{Fusion,2}$ on the channel dimension is to disperse the topological features and pixel class features into each subspace so that each partition set focuses on the feature changes in the current subspace domain. Because the pixel

category features in different subspace domains are highly correlated, the topological features have various degrees of implication. Therefore, based on this feature, when each subspace is updated with feature values through network training, each subspace can gradually learn how to enhance the pixel category features of each channel with the help of different degrees of topological features. In this process, different subspaces also gradually learn different topological features. Finally, the topological information and pixel category information embedded in $F_{Fusion,2}$ is naturally obtained by stacking all subspaces.

As shown in Fig. 4, the weighted excitation $W_{Fusion,2}$ for each channel of $F_{Fusion,2}$ is first obtained. The $F_{Fusion,2}$ of multi-modal feature fusion was globally averaged and pooled in spatial dimension to obtain 1×1 feature maps of C channels. Then, the result of global average pooling is fed into the subsequent simple multilayer perceptron composed of 1×1 convolution and activation function, which is used to learn the importance of C channels, namely the weight excitation of channels. $F_{Fusion,2}$ containing C channels was divided into k groups, each group containing C/k different channels $\{F_{k,1}, F_{k,2}, \ldots\}$, this process completes the partition of the subspace, and its corresponding channel excitations are also divided into k groups $\{W_{k,1}, W_{k,2}, \ldots\}$ are input to the feature decoupling module. The channel and pixel position attention mechanisms were operated on multiple channel features within each group to capture the correlations within and between feature maps. This is added to the initial weighted excitation $W_{k,i}$. The final output is recorded by 1×1 convolution and connected with $F_{k,i}$ residuals. Finally, the feature channels obtained from all subspaces are stacked to achieve the integration of information from multiple subspaces.

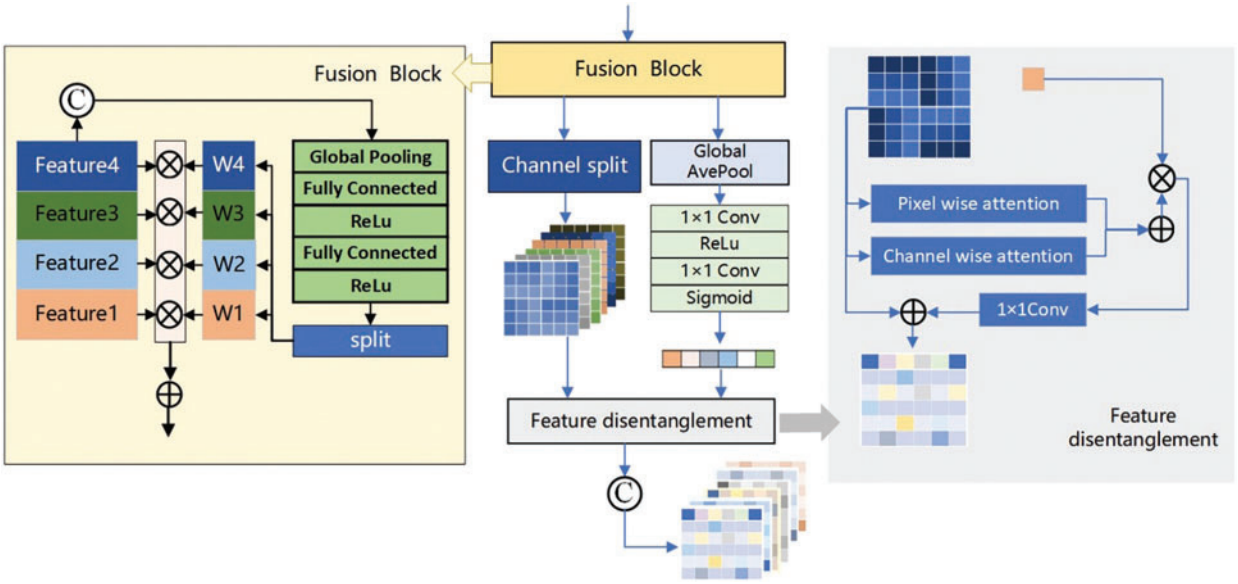

Figure 4: Feature decoupling structure

3.3 Decoder Structure

When medical images pass through each encoder level, the extracted features contain specific topological properties. To ensure that the topological properties of each level are fully utilized, we propose a decoder that can perform feature fusion. As shown in Fig. 5, the input of the decoder is divided into two parts. One part we call high-level features F_{main}, which are used for pixel classification.

Some of them are called topological attributes $F_{topology}$, which are used to characterize the relationship between pixels and surrounding neighborhoods.

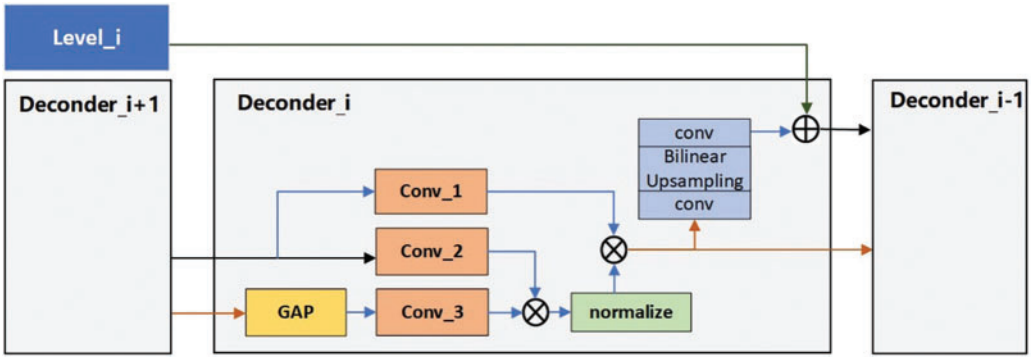

Figure 5: Decoder Structure structure

When $i = 4$, that is, when the feature information flows into the first feature decoder, we initialize F_{main} and $F_{topology}$ to F_{dis} (F_{dis} is the feature output of the decoupled module), and they will be updated iteratively in the subsequent decoding process. Firstly, the topology attribute feature $F_{topology}$ is enhanced by global average pooling, and then it and the high-level feature F_{main} are mapped into a shared manifold by 1×1 convolution.

$$F_{t,1} = Conv\_3(F_{topology}) \tag{13}$$

$$F_{m,1} = Conv\_2(F_{main}) \tag{14}$$

$$F_{t,m} = normalize(F_{t,1} \otimes F_{m,1}) \tag{15}$$

where, $F_{topology}$ represents the topological attribute feature, obtained by passing through 3×3 convolutional layers to obtain $F_{t,1}$. F_{main} represents high-level features passed through 2×2 convolutional layers to obtain $F_{m,1}$. The similarity between the mapped $F_{t,1}$ and $F_{m,1}$ is calculated by channel dot product, and then the regularization function is integrated to obtain the regularized category-direction attention feature map $F_{t,m}$. The attention feature map enhances direction-related features across channels, and irrelevant features are suppressed across channels. Furthermore, we use the attention feature map to improve the direction information of the high-level feature F_{main} by dot multiplication. Then, the features of the encoder output are added with the help of an upsampling operation.

$$F'_{topology} = Conv\_1(F_{main}) \otimes F_{t,m} \tag{16}$$

$$F'_{main} = F'_{topology} + Conv(Upsampling(Conv(F'_{topology}))) \tag{17}$$

The attention feature map $F_{t,m}$ is multiplied with the F_{main} processed by a 1×1 convolutional layer to obtain $F'_{topology}$. F'_{main} is obtained by adding $F'_{topology}$ together with $F'_{topology}$ after the convolution layer, upsampling, and convolution layer processing. $F'_{topology}$ and F'_{main}, respectively represent the topological attribute features and high-level features after the above processing, which are also the input of the next layer decoder. Through the above operation, the direction information is effectively fused into the space of the high-level feature stream, and the feature information from different levels of the encoder is effectively fused.

3.4 Loss Function

For medical images, system noise caused by device type and information loss caused by data transmission will cause different degrees of impact on image quality. From the perspective of imaging, although it will not affect human vision in discriminant decision-making, from the perspective of the model, the addition of noise and other disturbances will introduce information that is not related to the decision, affect the data distribution, and then degrade the performance of the model. To avoid the interference of redundant information on the accuracy of the segmentation network, the loss function is constructed based on the information bottleneck theory.

The Information Bottleneck (IB) theory understands the neural network as an encoder and a decoder; the encoder encodes the data into features, and the decoder decodes the features into the output. Its essence maximizes the mutual information between features and production and reduces the information between input and features. To retain the information most relevant to the input and the task. Information bottleneck theory definition:

$$R_{IB}(\theta) = I(Z, Y; \theta) - \beta I(Z, X; \theta) \tag{18}$$

where, $R_{IB}(\theta)$ represents the information bottleneck, θ represents the network parameters, $I(Z, Y; \theta)$ represents the mutual information between the output Y and the feature Z, $I(Z, X; \theta)$ represents the mutual information between the input and the feature Z.

The experience of Jia et al. [18] shows that using IB as the objective function of Deep Neural Network (DNN) learning will indeed increase the robustness of the model and reduce the sensitivity of feature extraction to input disturbances. However, the calculation of IB is very complex and cumbersome, and researchers use the Hilbert-Schmidt Independence Criterion (HSIC) as a practical computational alternative to IB. HSIC, a statistical dependence measure proposed by Gretton, is the Hilbert-Schmidt norm of the cross-covariance operator between distributions in the reproducing kernel Hilbert space. Like mutual information, HSIC captures the nonlinear dependence between random variables. Loss constraints on multimodal features based on HSIC can ensure a strong correlation between features and tasks and remove redundancy, which is defined as:

$$\begin{aligned} HSIC(X, Y) = {} & \mathrm{E}[k_X(X, X')\, k_{Y'}(Y, Y')] + \mathrm{E}[k_X(X, X')]\,\mathrm{E}[k_Y(Y, Y')] \\ & - 2\mathrm{E}[\mathrm{E}[k_X(X, X')]\,\mathrm{E}[k_Y(Y, Y')]] \end{aligned} \tag{19}$$

where, k denotes the kernel function, X and Y are two random variables, and X' and Y' denote the transpose of X and Y. E is the expectation. As a variant of the more classical information Bottleneck, proposed the Hilbert-Schmidt information bottleneck (HSIC Bottleneck), which is defined as follows:

$$R_{HB}(\theta) = HSIC(Z, Y; \theta) - \beta HSIC(Z, X; \theta) \tag{20}$$

where, $R_{HB}(\theta)$ represents the Hilbert-Schmidt information bottleneck, $HSIC(Z, Y; \theta)$ represents the independence criterion between feature Z and target task Y, $HSIC(Z, X; \theta)$ denotes the independence criterion between feature Z and input data X, θ denotes the network parameters, and β is the hyperparameter.

Based on the above analysis, we re-examine the HSIC Bottleneck. When extracting cross-modal information, we take it as part of the constraints of multi-modal feature information. Firstly, we ensure that the features extracted from each layer of the network are as highly relevant to the task as possible, and secondly, we ensure that the feature information is unique and shared between modes. Finally, the redundancy of feature information is reduced to ensure that the information contained in the feature map can serve the downstream tasks to the greatest extent, reduce the interference of redundant

information, and increase the model's learning ability and generalization ability. The characteristic loss function based on HSIC Bottleneck is defined as follows:

$$L_{HSIC} = \alpha \sum_{i=1}^{4} \sum_{l=1}^{L} [HSIC(X_i, Z_{i,l})] - \beta \sum_{i=1}^{4} \sum_{l=1}^{L} [HSIC(Y, Z_{i,l})] \tag{21}$$

where, the setting of hyperparameters is empirically selected according to reference, where $\alpha = 0.001$, $\beta = 0.0005$. i represents the ith mode, and $i = \{1, 2, 3, 4\}$ corresponds to the four modes of MMRI. l represents the first layer, and $l = \{1, 2, 3, 4\}$ corresponds to the four levels of the encoder. X represents the input image, Z represents the feature, and Y represents the target task. By constraining the loss of multimodal features, the strong correlation between features and tasks is ensured, redundancy is removed, and the interference of redundant information on feature extraction is reduced.

Multimodal images are different descriptions of the same target. MRI images with other modalities have different representation advantages for the lesion area, with the uniqueness and sharing of information between modalities. When multimodal data is combined with a specific task, the information contained in the data is first classified: one is the information shared between different modalities related to the task, one is the information that is unique to each modality about the task, and the last is the redundant information that is not associated with the task. Three kinds of information are defined based on mutual information:

(1) All the mutual information between all modal data and tasks.

$$\begin{aligned} I(X_1, X_2, X_3, X_4; Y) = {} & I(X_1; X_2; X_3; X_4; Y) + I(X_1; Y|X_2, X_3, X_4) + I(X_2; Y|X_1, X_3, X_4) \\ & + I(X_3; Y|X_1, X_2, X_4) + I(X_4; Y|X_1, X_2, X_3) \end{aligned} \tag{22}$$

where,

$$I(X_1, X_2, X_3, X_4; Y) = \int \ldots \int p(x_1, x_2, x_3, x_4, y) log \frac{p(x_1, x_2, x_3, x_4, y)}{p(x_1, x_2, x_3, x_4)\, p(y)} dx_1 dx_2 dx_3 dx_4 dy \tag{23}$$

where, denote all mutual information between joint random variables X_1, X_2, X_3, X_4 and task Y. $I(X_1; Y|X_2, X_3, X_4)$ denotes information unique to task-related X_1 modes, $I(X_2; Y|X_1, X_3, X_4)$ denotes task-related information unique to X_2 modes, $I(X_3; Y|X_1, X_2, X_4)$ denotes information unique to X_3 modes relevant to the task, and $I(X_4; Y|X_1, X_2, X_3)$ denotes information unique to the mode X_4 associated with the task.

(2) Shared and unique information related to modality and task.

$$\begin{aligned} I(X_1; X_2; X_3; X_4; Y) &= I(X_1; X_2; X_3; X_4) - I(X_1; X_2; X_3; X_4|Y) \\ &= \int \ldots \int p(x_1, x_2, x_3, x_4)\, log \frac{p(x_1, x_2, x_3, x_4)}{p(x_1)\, p(x_2)\, p(x_3)\, p(x_4)} dx_1 dx_2 dx_3 dx_4 \\ &\quad - I(X_1; X_2; X_3; X_4|Y) \end{aligned} \tag{24}$$

$$I(X_1; X_2; X_3; X_4|Y) = \int \ldots \int p(x_1, x_2, x_3, x_4|y)\, log \frac{p(x_1, x_2, x_3, x_4|y)}{p(x_1|y)\, p(x_2|y)\, p(x_3|y)\, p(x_4|y)} dx_1 dx_2 dx_3 dx_4 dy \tag{25}$$

where, $I(X_1; X_2; X_3; X_4; Y)$ represents the task-related shared information, and $I(X_1; X_2; X_3; X_4)$ represents the shared information between modes, $I(X_1; X_2; X_3; X_4|Y)$ denotes shared information that is not relevant to the task. The proposed model is assumed to be $f(\theta)$, and the ability of $f(\theta)$ to extract

task-related shared features Z_s and unique features Z_u from multimodal data is expected to be obtained by training.

$$Z_{s,i,l} = \underset{Z_{i,l}}{\operatorname{argmax}}\, I\left(Z_{i,l}; X_{-i}; Y\right) \tag{26}$$

$$Z_{u,i,l} = \underset{Z_{i,l}}{\operatorname{argmax}}\, I\left(Z_{i,l}; Y|X_{-i}\right) \tag{27}$$

where, $i = \{1, 2, 3, 4\}$ corresponds to the four modes of MMRI, $l = \{1, 2, 3, 4\}$ corresponds to the four levels of encoder, and $Z_{i,l}$ represents the features generated by mode X_i in the Lst-layer network coding. $Z_{s,i,l}$ represents task-relevant features extracted from the X_i modality and produced by the lth layer network that are shared with other modalities simultaneously, and X_{-i} represents all other modalities that are unexpected from the X_i modality. $Z_{u,i,l}$ represents the task-relevant and mode-unique features extracted from X_i modes and generated by the L-layer network.

In view of this, the multi-modal feature loss function based on mutual information is defined as follows:

$$L_{\text{Multi}} = 1 - \sum_{i=1}^{4}\sum_{l=1}^{L}\left[I\left(Z_{i,l}; X_{-i}; Y\right) + I\left(Z_{i,l}; Y|X_{-i}\right)\right] \tag{28}$$

Loss constraints on multimodal features decouple the task-related unique information and shared information. The effective representation of multimodal feature information is enhanced by maximizing task-related unique information and shared information and minimizing task-irrelevant redundant information. Starting from this idea, we establish the loss function based on HSIC and mutual information as follows:

$$L = L_{dice} + L_{cross-entropy} + L_{\text{Multi}} + L_{HSIC} \tag{29}$$

where, L_{dice} is the Dice loss of image segmentation, and $L_{cross-entropy}$ is the cross-entropy loss.

4 Experimental Result

4.1 Experimental Detail

This paper was carried out in a hardware environment with an Intel® Core™i9-10900X CPU and an NVIDIA Geforce GTX Titan A100 GPU. The network model is based on the PyTorch framework, Torch version 1.10.2, Cuda version 11.3, and Python version 3.8.10. The model was trained using the Adam optimizer after 300 iterations. The initial learning rate was set to 0.0001, the weight decay to 0.0005, the batch size to 16, and the patch size to 128×128.

To quantitatively evaluate the proposed method, the Dice coefficient, and HD95 were selected as the evaluation indexes of all segmentation algorithms. Dice is a set similarity measure function commonly used to calculate the similarity between labels and segmentation results. A more considerable Dice value indicates better segmentation. HD95 determines the Hausdorff distance between labels and segmentation results. The smaller the HD95 value, the better the segmentation effect.

The training and testing experiments are carried out on the BraTs2021 dataset to verify the algorithm's effectiveness proposed in this paper. The effectiveness of the proposed algorithm is further verified on the ANNLIB dataset. Further, to confirm the generalization performance of the proposed algorithm, the trained model is directly used in the test experiment of BraTs2023-MET. Among them, the Tumor segmentation labels of the BraTs2021 dataset included background, Edema (ED), Necrosis and Non-Enhancing Tumor (NCR/NET), and Enhancing Tumor (ET). The purpose of the

segmentation task in this chapter is to segment the Whole Tumor (WT), Enhancing Tumor (ET), and Tumor Core (TC) regions.

4.2 Ablation Experiments

Ablation studies were performed on the BraTS2021 dataset to evaluate the contribution of the main modules in the methodology. The baseline method is set as follows: the feature decoupling module is replaced by a simple feature stacking method for feature fusion, the decoder uses a simple convolution combination method for feature decoding, and the loss function uses the most straightforward Dice loss and cross-entropy loss weighting. The ablation experiments of four modules (loss function L_{Multi}, loss function L_{HSIC}, feature decoupling module, and decoder) were carried out successively to observe the effects of the above four modules on the model performance.

It can be found from Table 1 that the segmentation results of FDIBMNet reached the optimal in terms of Dice and HD95 in WT, TC, and ET. The effect of the decoder on the whole model was investigated. The ablation experiment showed that the HD95 of WT reached 62.628, the Dice of TC reached 0.829, the Dice of ET was 0.787, and the HD95 was 44.420, all of which achieved suboptimal results. However, although the tumor segmentation effect was practical, it was still not as good as the proposed FDIBMNet model. Considering the impact of L_{Multi} loss function on the proposed model, the segmentation performance of the proposed model deteriorates sharply, and the segmentation of TC and ET regions is close to the baseline model, which indicates that L_{Multi} seriously affects the segmentation effect. Decoupling task-related unique and shared information is crucial to the model's performance. The absence of the loss function L_{HSIC} reduces the model's overall performance by more than 0.15 in the Dice score. The essence of L_{HSIC} is to ensure.

Table 1: Results of ablation experiments on the BraTs2021 dataset

Method	WT		TC		ET	
	Dice↑	HD95↓	Dice↑	HD95↓	Dice↑	HD95↓
Baseline	0.523	139.718	0.629	93.228	0.636	91.998
Ours $-$ L_{Multi}	0.615	104.811	0.639	93.640	0.655	90.411
Ours $-$ L_{HSIC}	**0.806**	51.489	0.734	**41.197**	0.724	66.213
Ours-feature disentanglement	0.715	62.695	0.747	49.536	0.753	47.972
Ours-decoder	0.774	**62.628**	**0.829**	48.715	**0.787**	**44.420**
Ours	**0.896**	**32.300**	**0.861**	**37.308**	**0.854**	**38.220**

Note: For a given task, ↑ indicates that larger values are better, ↓ indicates that smaller values are better, the red subject represents the model with the best performance, and the blue subject represents the model with the second best performance.

In the feature disentanglement module, the information stacked matrix after the fusion of four modes is input. Through the combination of global pooling, full connection and activation function, the excitation weights of multiple channels in the full mode are obtained, and then the initial dimension reduction work is completed through channel selection and global average pooling. The results were input into the Pixel wise attention and Channel Wise attention of the feature decoupling module to complete the feature decoupling. The results of ablation experiments combined with the network framework to remove the feature decoupler module showed that the Dice of the model decreased by 0.181, 0.082, and 0.101, and the HD95 increased by 30.395, 12.228, and 9.752, respectively. This result indicates that the feature decoupling module can effectively influence the results of the network on the

segmentation task. At the same time, to further understand the basic situation of the algorithm, we calculated the number of parameters and floating-point numbers of different structures, as shown in Table 2.

Table 2: Computational complexity of algorithms

Module	Encoder block	Disentanglement block	Deconder block	Total
Para. (M)	6.69	2.3	12.84	21.79
FLOPs	75.49 G			

To better prove the convergence of the algorithm proposed in this paper, the epoch of BraTs2021 data set is plotted with the change of loss. Based on Fig. 6, it can be found that after removing the Dice module, the loss function gradually converges when the epoch = 10. After removing the Cross-entropy module, the loss function converges gradually after epoch = 15, and after removing the multimodal fusion module, the loss function converges gradually after epoch = 8. After removing the HSIC module, the loss function gradually converges after the epoch = 9. The convergence of the algorithm is proved.

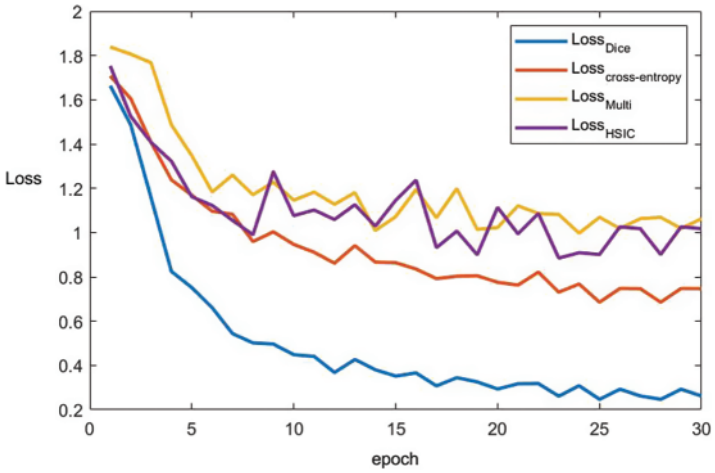

Figure 6: The convergence curve of each loss term

4.3 Contrast Experiments

To verify the effectiveness of the proposed method more comprehensively, this paper selects seven segmentation methods that have performed well in the field of multimodal medical image segmentation in recent years for comparative experiments. It includes multimodal medical image segmentation methods based on the CNN framework, multimodal medical image segmentation methods based on the GAN framework, and multimodal medical image segmentation methods based on the Transformer framework Table 3, and the experimental results are presented and analyzed from the perspective of quantitative experiment and qualitative experiment.

Table 3: Comparison of different methods in medical image segmentation

Category	Methods	Characteristic
CNN	AACNN (2023)	The axial attention is introduced into CNN to capture semantic information, and deep supervision and mixed loss are used to deal with category imbalance, which improves the segmentation performance.
	ESAB (2023)	Segmentation method based on fusion of deep semantic and edge information in MMRI.
	nnUNet (2020)	By configuring the segmentation pipeline with fixed parameters, rule-based parameters and empirical parameters, the automated configuration process enables nnUNet to adapt to a variety of different medical image segmentation tasks.
GAN	DualMMP-GAN (2022)	Patches were used to represent lesions of different sizes, and perceptual consistency loss was used to learn the mapping relationship between the generated modality and the target modality at different semantic levels.
	CycleGAN (2023)	Transfer learning techniques are used to inject valuable features into the network.
Transformer	UNETR (2022)	Pure Transformers are used as encoders to learn the sequence representation of the input and to efficiently capture global multiscale information.
	NestedFormer (2022)	A nested Transformer was used to establish the long-range intra- and inter-modal dependence of MMRI for brain tumor segmentation.
	BTSwin-U-Net (2023)	3D U-shaped symmetric brain tumor segmentation network based on Swin Transformer to solve the problem of scarce training data.
	CIML (2024)	Task decomposition is used to reduce the information dependence between modalities, and a message passing mechanism is used to extract non-redundant information from other modalities. Inspired by the variational information bottleneck, this framework transforms redundant filtering into complementary information learning and is implemented through variational inference and cross-modal spatial attention mechanisms.

Table 4 reports the experimental results of the seven methods and the method proposed in this chapter on the BraTS2021 dataset under the same experimental environment. FDIBMNet was optimal in Dice and HD95 of WT, TC, and ET. Combining the results of Table 4 and Fig. 7 can be found, compared with the method based on the CNN framework, the Dice of FDIBMNet in WT, TC, and ET were increased by 0.130, 0.074, and 0.083 on average, and the HD95 were decreased by 27.980, 20.323, and 31.252 on average. Compared with the CNN framework, the information flow and feature fusion of FDIBMNet ensure the richness of information in the downsampling step, which

can improve the accuracy of image segmentation and reduce the distance between the target region and the segmentation region. Compared with the method based on the GAN framework, the Dice of FDIBMNet in WT, TC, and ET were increased by 0.115, 0.108, and 0.105 on average, and the HD95 decreased by 17.451, 31.486, and 33.933 on average. Compared with the GAN framework, the feature decoupling and topological attribute features of FDIBMNet ensure the quality of the information in the upsampling step, which is conducive to mapping the segmentation results back to the source image. Compared with the method based on the Transformer framework, the Dice of FDIBMNet in WT, TC, and ET were increased by 0.113, 0.080, and 0.071 on average, and the HD95 were decreased by 23.123, 18.557, and 23.065 on average. Like the Transformer framework, FDIBMNet captures multi-scale features and solves the feature relationships within and between modes through information flow. The difference is that FDIBMNet adopts a parallel structure in the down-sampling step, which retains topological attributes and high-level features. This is conducive to improving the effect of medical image segmentation. According to the results of the quantitative analysis, FDIBMNet is significantly better than CNN, GAN, and Transformer in terms of the segmentation effect of WT, TC, and ET of brain tumors.

Table 4: The comparative experimental results of different algorithms in BraTs2021 dataset

Categories	Methods	WT		TC		ET	
		Dice↑	HD95↓	Dice↑	HD95↓	Dice↑	HD95↓
CNN	AACNN	0.704	84.441	0.728	79.639	0.725	79.484
	ESAB	0.779	48.898	0.798	52.384	0.753	71.952
	nnUNet	0.816	47.502	0.835	40.871	0.834	56.981
GAN	DualMMP-GAN	0.763	54.190	0.750	73.564	0.748	74.816
	CycleGAN	0.799	45.311	0.756	64.023	0.750	69.490
Transformer	UNETR	0.768	54.467	0.742	71.189	0.731	76.181
	NestedFormer	0.702	82.716	0.724	75.707	0.727	74.102
	BTSwin-U-Net	**0.843**	**38.708**	**0.851**	**38.104**	0.832	**45.355**
	CIML	0.818	45.800	0.808	38.560	**0.843**	49.503
Ours	Ours	**0.896**	**32.300**	**0.861**	**37.308**	**0.854**	**38.220**

Note: For a given task, ↑ indicates that larger values are better, ↓ indicates that smaller values are better, the red subject represents the model with the best performance, and the blue subject represents the model with the second best performance.

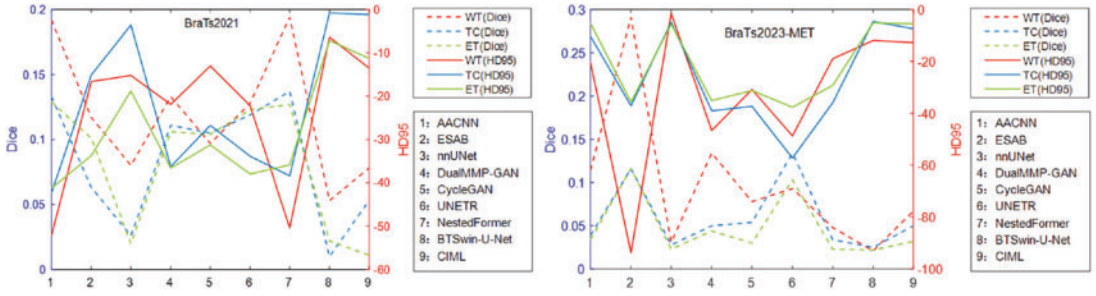

(a) BraTs2021 (b) ANNLIB

Figure 7: Line plot of the error of BraTs2021 and ANNLIB results

Qualitative analysis was performed using visualization to judge FDIBMNet's effect further. In this chapter, two sample images are selected to visually compare the impact of different methods on the segmentation task. Fig. 8 shows the segmentation results of brain tumor slices, labels, and techniques. In the source image, the brain tumor was not significantly imaged in the T1WI mode, and there was no noticeable pixel difference from the surrounding tissue. In the FLAIR mode, the edema area was very significant and had a clear boundary with the surrounding tissue, but the tumor core and the enhanced tumor pixel area were concealed, which was challenging to distinguish significantly. In T1Gd mode, only the tumor core and enhanced tumor showed pixel intensity that differed from other tissues, and there was a clear boundary between them. The appearance of the whole tumor was clear on T2WI.

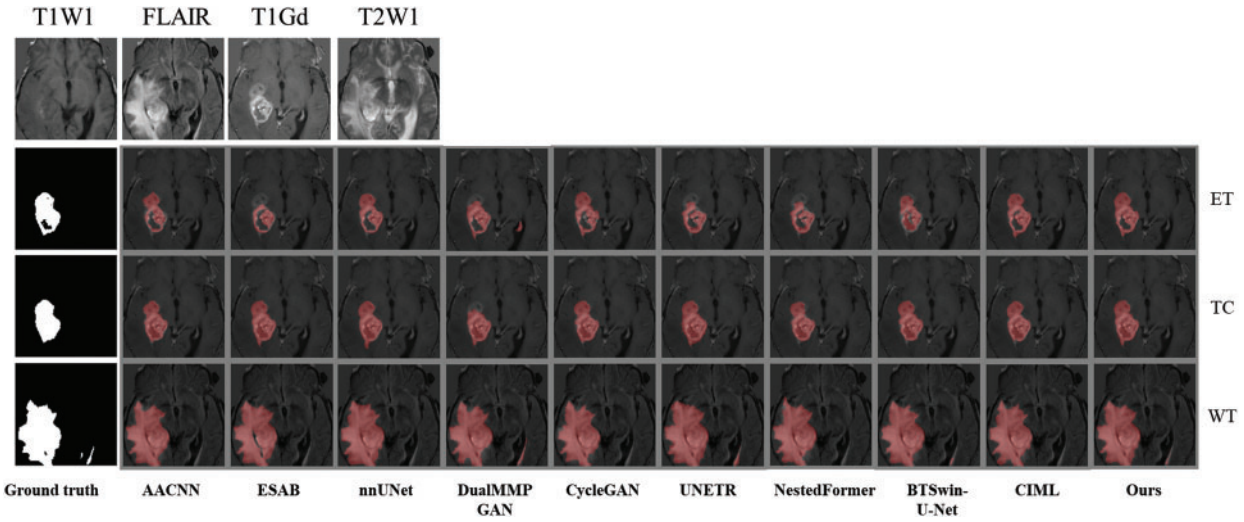

Figure 8: The first example picture contrast method visualizes the results

Combined with Fig. 9, it is found that the medical image segmentation method based on the CNN framework has a poor processing effect on the incoherent lesion area. For example, there are non-tumor areas inside the enhanced tumor area of the first example, and the segmentation effect of the CNN framework on this part is poor, with the phenomenon of under segmentation. At the same time, the boundary segmentation of the tumor core and all tumors was not precise. From the perspective of the network framework, the two methods based on CNN did not enhance the boundary information, resulting in unclear boundaries. The medical image segmentation method based on the GAN framework has a better processing effect on incoherent regions than CNN. The main reason for this phenomenon is that the GAN-based method can extract semantic information at different scales, ensuring the multi-scale richness of information, but a certain degree of boundary still needs to be added. Medical image segmentation methods based on the Transformer framework have poor processing effects on incoherent regions and boundaries. For example, the NestedFormer and BTSvin-U-Net methods in the second example think that there are non-tumor regions in the center of the tumor. The UNETR method showed poor segmentation of the left lower area of all tumors. Although the medical image segmentation method based on the Transformer framework considers the multi-scale information within modalities and the spatial information between modalities, its loss function does not constrain the information. It cannot achieve the effect of accurate segmentation. The FDIBMNet method proposed in this chapter can accurately segment the non-tumor regions inside the tumor and segment the boundaries of the cancer with a good segmentation effect.

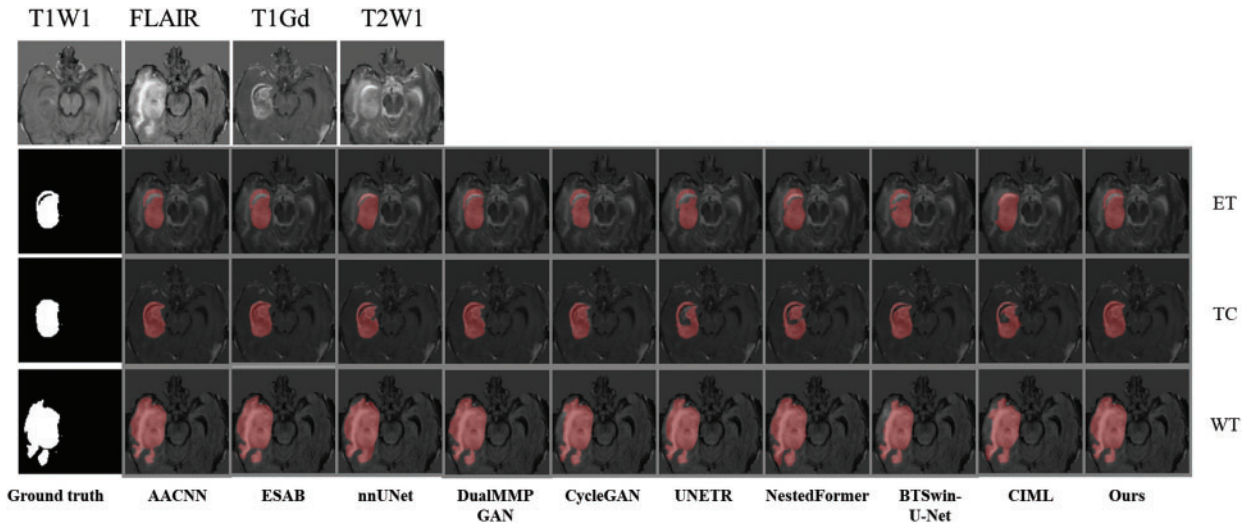

Figure 9: The second example picture contrast method visualizes the results

To better verify the effectiveness of the algorithm, ANNLIB dataset was used to further verify the effectiveness of the algorithm. According to the results in Table 5, it can be found that our proposed method achieves the optimum in both Dice and HD95 indices, in which nnUNet achieves the second-best. Combined with the line chart results, the Dice index was increased by 0.098 on average, and the HD95 index was decreased by 37.936 on average, which further verified the effectiveness of the FDIBMNet method.

Table 5: The comparative experimental results of different algorithms in ANNLIB dataset

Categories	Methods	Dice↑	HD95↓
CNN	AACNN	0.772	86.158
	ESAB	0.717	68.776
	nnUNet	**0.905**	**36.588**
GAN	DualMMP-GAN	0.821	72.789
	CycleGAN	0.864	71.835
Transformer	UNETR	0.809	40.029
	NestedFormer	0.821	71.636
	BTSwin-U-Net	0.869	79.528
	CIML	0.857	87.796

The experimental results of qualitative analysis and quantitative analysis show that the CNN-based image segmentation method could be more friendly to boundary segmentation. The image segmentation method based on the Transformer will segment the tumor area into non-tumor areas prone to undersegmentation. The image segmentation method based on GAN has a better effect than CNN and Transformer, but there is still a certain degree of clarity. Due to the feature decoupling module, the FDIBMNet method proposed in this paper extracts the topological attribute features,

ensuring incoherent lesion regions' segmentation effect. In addition, information flow and fusion combined with mutual information loss function safeguard the richness of information and the extraction of crucial details, thereby improving the performance of the overall segmentation model.

4.4 Generalization Experiments

The trained model based on the BraTS2021 glioma dataset was directly used in the brain metastases segmentation test task of the BraTS2023-MET dataset to verify the generalization of the method proposed in this chapter. The experimental results of Dice and HD95 for all network methods are listed in Table 6 and Fig. 10.

Table 6: The comparative experimental results of different algorithms in BraTS2023-MET dataset

Categories	Methods	WT		TC		ET	
		Dice↑	HD95↓	Dice↑	HD95↓	Dice↑	HD95↓
CNN	AACNN	0.682	55.992	0.707	44.264	0.710	43.908
	ESAB	0.505	129.283	0.630	71.007	0.628	74.129
	nnUNet	0.765	37.001	0.718	38.833	0.721	44.172
GAN	DualMMP-GAN	0.662	82.118	0.696	72.951	0.700	73.603
	CycleGAN	0.718	66.322	0.692	71.188	0.714	69.734
Transformer	UNETR	0.703	84.177	0.612	91.199	0.641	76.181
	NestedFormer	0.748	54.470	0.712	69.832	0.721	67.757
	BTSwin-U-Net	**0.775**	**47.435**	**0.721**	**38.548**	**0.722**	**43.682**
	CIML	0.729	48.244	0.696	41.328	0.712	44.029
Ours	Ours	**0.796**	**35.537**	**0.746**	**33.957**	**0.744**	**38.559**

Note: For a given task, ↑ indicates that larger values are better, ↓ indicates that smaller values are better, the red subject represents the model with the best performance, and the blue subject represents the model with the second best performance.

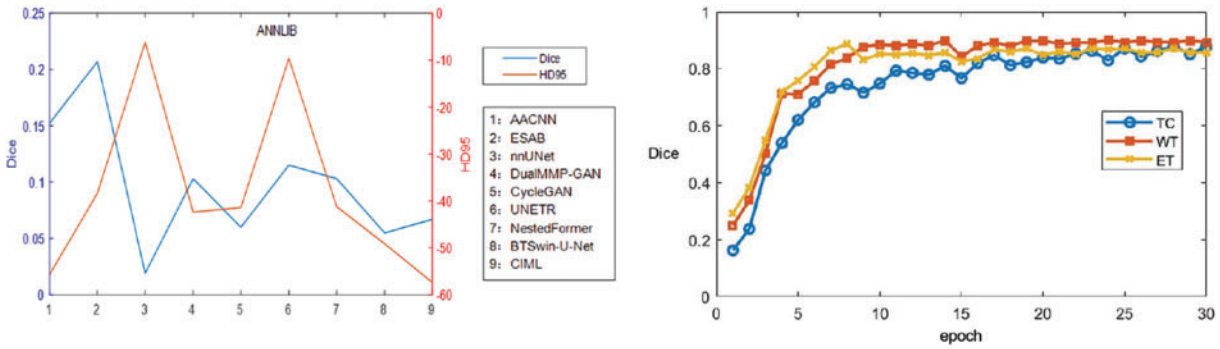

(a) Error curve (b) Convergence curve

Figure 10: Line plot of the error of BraTS2023-MET results and the convergence curve of Dice of WT, TC, WT

Table 6 and Fig. 10 report the experimental results obtained by the abovementioned methods on the BraTS2023-MET dataset under the same experimental environment. The Dice index of

FDIBMNet in the three WT regions, TC regions, and ET regions was 0.796, 0.746, and 0.744, respectively, and the HD95 index was 35.537, 33.957, and 38.559, respectively, which were all optimal values. Compared with the method based on the CNN framework, the Dice scores of FDIBMNet in WT, TC, and ET were increased by 0.145, 0.061, and 0.058 on average, and the Dice scores of HD95 were decreased by 38.555, 17.411, and 15.511 on average, with the most significant performance improvement. Compared with the method based on the GAN framework, the Dice of FDIBMNet in WT, TC, and ET were increased by 0.106, 0.052, and 0.037 on average, and the HD95 were decreased by 38.683, 38.113, and 33.110 on average. Compared with the method under the Transformer framework, the Dice of FDIBMNet in WT, TC, and ET were increased by 0.057, 0.061, and 0.045 on average, and the HD95 were decreased by 23.045, 26.270, and 19.353 on average. On the BraTs2021 dataset, the GAN-based image segmentation method is significantly better than the CNN-based image segmentation method, and the opposite is observed on the BraTS2023-MET dataset. The reason is that the T1Gd modality is missing in the generalization dataset, so the information on the lesion is relatively less, which is not enough to describe the disease state. On the BraTs2021 dataset and BraTS2023-MET dataset, the FDIBMNet method showed the best performance, and this result further verified the segmentation performance of the FDIBMNet method.

To better prove the generalization of the algorithm proposed in this paper, a graph of the change of epoch with Dice of the BraTS2023-MET dataset is drawn as Fig. 10b. Based on the graph, it can be found that when the TC, WT, and ET regions are divided, the Dice gradually converges when the epoch = 15. The generalization of the algorithm is proved.

Qualitative analysis was performed using visualization to judge the generalization effect of FDIBMNet further. In this section, an example image is selected to visually compare the impact of different methods on the segmentation task. According to the visualization results Fig. 11, ESAB and UNETR judged the brighter pixel area in the imaging as the lesion area. Methods BTSLOU-U-NET classifies all tumors with dark pixels as usual, and most of the pixels with strong pixels as tumors, which will lead to misdiagnosis or missed diagnosis. However, the WT region, TC region, and ET region can be segmented relatively entirely by the method proposed in this paper, and the normal tissue is rarely misclassified as the lesion area, reducing misdiagnosis. In particular, the segmentation effect is suitable for regions with blurred edges and strong pixels, showing good anti-interference ability. This is because FDIBMNet emphasizes the decoupling of multimodal information, directional information, and category information so that the extracted information can be directed to the lesion area with direction guidance and reduce the interference of pixel light and dark. In addition to inaccurate brain tumor detection, the ET and TC regions should be included in the WT region, but the BTWCN-U-NET method shows that the WT region does not contain the TC region. The visualization experimental results of the method proposed in this chapter show that FDIBMNet can effectively capture robust correlation information with the help of the L_{HSIC} loss function, which ensures that the ET region and TC region are included in the WT region, which is consistent with the actual situation of brain tumor detection and segmentation.

By combining the quantitative and qualitative analysis of the generalization experiment, FDIBM-Net flows the information between different modes through the bottom-up flow, combines the mutual information and the information bottleneck loss function, and ensures the adequate flow of information and improves the quality of feature extraction. The feature decoupling method can effectively obtain high-level features and topological attributes of image segmentation, and with the parallel upsampling structure, the accurate segmentation of incoherent lesion regions and lesion boundaries can be ensured.

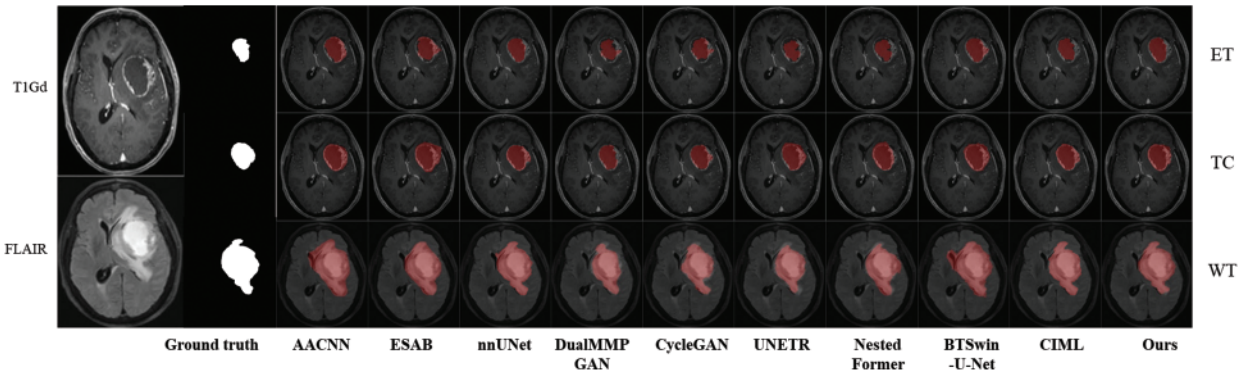

Figure 11: Generalization of experimental results

4.5 Hyperparametric Analysis

We drew the pre-experiment loss function curve to determine the number of training rounds and found that FDIBMNet began to decline smoothly when Epoch was 50 and became stable around Epoch 100. Therefore, Epoch 100 was selected for formal experiments in this paper (Fig. 12).

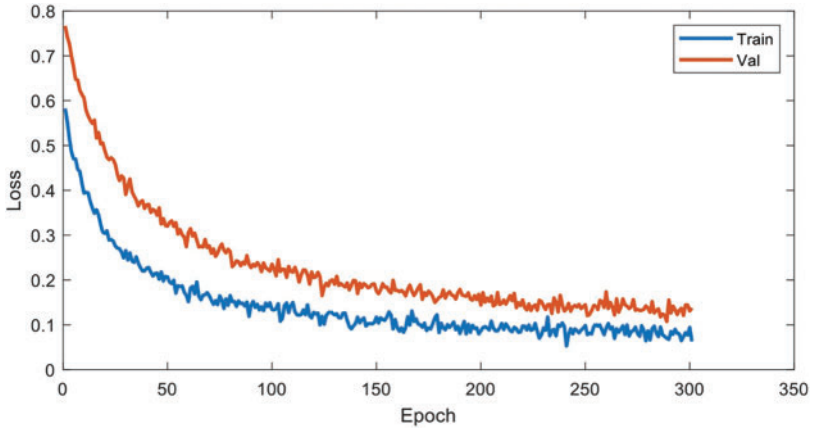

Figure 12: Hyperparametric analysis

5 Conclusion

This paper proposes a novel multimodal segmentation framework for brain tumors based on feature decoupling and information bottleneck theory (FDIBMNet). The proposed framework contains a multi-branch encoding structure, a feature decoupler, and a two-branch decoding structure. Firstly, based on INNs, a multi-direction flow and multi-branch encoder with bottom-up and intermodal information interaction was constructed, and a "complete" "representation space" was built to maximize the information that contributed and correlated to the task and suppress the information that did not contribute and correlated to the task or interfered with the task. Secondly, based on the topological properties of medical images (pixel connectivity and adjacency), a feature decoupling module was designed to decouple the relationship between pixels and geometric attributes of medical image features from the feature space and to model and enhance the topological attribute representation between interested pixels. From the information bottleneck, loss constraints are applied to multimodal

features to ensure a strong correlation between features and tasks and remove redundancy. Finally, based on the mutual information constraint between the input and output, the sharing and uniqueness of multimodal features are decoupled, and the effectiveness and generalization of the proposed segmentation method are verified on BraTS2020 and BraTS2023-MET datasets. As a visualization task of segmentation results, this paper can combine image fusion and image classification tasks to form a multimodal and multi-task medical image auxiliary diagnosis system for brain tumors. Accurate brain tumor segmentation can help doctors better understand the location, size and morphology of tumors, to develop more precise treatment plans and reduce the damage to healthy brain tissue. In addition, multimodal methods can integrate information from different imaging modalities, such as structural information, functional information and metabolic information, to provide a more comprehensive description of tumor characteristics, which is of great significance for personalized medicine and precision medicine. Therefore, the research in this paper not only promotes the application of machine learning technology in the field of medical image processing, but also provides technical support for improving the efficacy and safety of brain tumor treatment. But there are still some shortcomings in this paper. With the continuous development of multimodal fusion technology, the multi-modal image fusion segmentation technology can be studied from the perspective of diffusion model. It is also possible to consider extending to large model directions.

Acknowledgement: We thank the National Natural Science Foundation of China for supporting this project. We would like to thank Li Yang for the guidance of this article. Thanks to Shanghai Zhangjiang Institute of Mathematics for the support of computing power.

Funding Statement: The manuscript was supported by the following grants: Beijing Natural Science Foundation (No. Z210003); National Natural Science Foundation of China (NSFC12026607); National Natural Science Foundation of China (NSFC12031016); Key R&D Program of the Scientific Research Department (2020YFA0712203); Key R&D Program of the Scientific Research Department (2020YFA0712201).

Author Contributions: Xuemei Yang: Data curation, Methodology, Software, Validation, Writing—original draft and review. Yuting Zhou: Conceptualization, Supervision, Writing—review and editing. Shiqi Liu: Data curation, Investigation, Visualization. Junping Yin: Conceptualization, Funding acquisition, Methodology, Resources, Supervision, Writing—review & editing. All authors reviewed the results and approved the final version of the manuscript.

Availability of Data and Materials: This article uses the public data sets are as follows: BraTS2021 (https://www.synapse.org/Synapse:syn25829067/wiki/610863) (accessed on 05 December 2024), BraTs2023-MET (https://www.synapse.org/Synapse:syn51156910/wiki/622553) (accessed on 05 December 2024), ANNLIB (https://www.med.harvard.edu/AANLIB/home.html) (accessed on 05 December 2024).

Ethics Approval: The relevant data ethics work in this paper has been approved by the Chinese Academy of Engineering Physics.

Conflicts of Interest: The authors declare no conflicts of interest to report regarding the present study.

References

[1] X. Li *et al.*, "Adversarial multimodal representation learning for click-through rate prediction," in *Proc. Web Conf. 2020 (WWW'20)*, New York, NY, USA, Association for Computing Machinery, 2020, pp. 827–836.

[2] S. Mai, Y. Zeng, and H. Hu, "Multimodal information bottleneck: Learning minimal sufficient unimodal and multimodal representations," *IEEE Trans. Multimed.*, vol. 25, pp. 4121–4134, 2023.

[3] C. Sun *et al.*, "Automatic segmentation of liver tumors from multiphase contrast-enhanced CT images based on FCNs," *Mach. Learn. Graph. Anal. Computat. Biomed.*, vol. 183, no. 3, pp. 58–66, 2017. doi: 10.1016/j.artmed.2017.03.008.

[4] A. Ben-Cohen, E. Klang, A. Kerpel, E. Konen, M. M. Amitai and H. Greenspan, "Fully convolutional network and sparsity-based dictionary learning for liver lesion detection in examinations," *Neurocomputing*, vol. 275, no. 9, pp. 1585–1594, 2018. doi: 10.1016/j.neucom.2017.10.001.

[5] Y. Feng *et al.*, "Multi-stage fully convolutional network for precise prostate segmentation in ultrasound images," *Biocyber. Biomed. Eng.*, vol. 43, no. 3, pp. 586–602, 2023. doi: 10.1016/j.bbe.2023.08.002.

[6] S. Chen *et al.*, "LD-UNet: A long-distance perceptual model for segmentation of blurred boundaries in medical images," *Comput. Biol. Med.*, vol. 171, no. 3, pp. 108–120, 2024. doi: 10.1016/j.compbiomed.2024.108120.

[7] C. Yu, Y. Wang, C. Tang, W. Feng, and J. Lv, "EU-Net: Automatic U-Net neural architecture search with differential evolutionary algorithm for medical image segmentation," *Comput. Biol. Med.*, vol. 167, no. 10, 2023, Art. no. 107579. doi: 10.1016/j.compbiomed.2023.107579.

[8] Z. Zhang, C. Wu, S. Coleman, and D. Kerr, "Dense-inception U-Net for medical image segmentation," *Comput. Methods Programs Biomed.*, vol. 192, no. 10, 2020, Art. no. 105395. doi: 10.1016/j.cmpb.2020.105395.

[9] Q. Jiang, H. Ye, B. Yang, and F. Cao, "Label-decoupled medical image segmentation with spatial-channel graph convolution and dual attention enhancement," *IEEE J. Biomed. Health Inform.*, vol. 28, no. 5, pp. 2830–2841, 2024. doi: 10.1109/JBHI.2024.3367756.

[10] Z. Zhang, Y. Wen, X. Zhang, and Q. Ma, "CI-UNet: Melding convnext and cross dimensional attention for robust medical image segmentation," *Biomed. Eng. Lett.*, vol. 14, no. 2, pp. 341–353, 2024. doi: 10.1007/s13534-023-00341-4.

[11] Y. Li, Y. Wu, M. Huang, Y. Zhang, and Z. Bai, "Attention-guided multi-scale learning network for automatic prostate and tumor segmentation on MRI," *Comput. Biol. Med.*, vol. 165, no. 1, 2023, Art. no. 107374. doi: 10.1016/j.compbiomed.2023.107374.

[12] H. Liu, M. Shao, Y. Qiao, Y. Wan, and D. Meng, "Unpaired image super-resolution using a lightweight invertible neural network," *Pattern Recognit.*, vol. 144, no. 2, 2023, Art. no. 109822. doi: 10.1016/j.patcog.2023.109822.

[13] L. Zhang, B. Verma, D. Stockwell, and S. Chowdhury, "Density weighted connectivity of grass pixels in image frames for biomass estimation," *Expert. Syst. Appl.*, vol. 101, no. 7, pp. 213–227, 2018. doi: 10.1016/j.eswa.2018.01.055.

[14] X. Wang, H. Liu, J. Zhu, Y. Sheng, and C. Zhang, "Deep multimodal medical image fusion network based on high and low frequency feature decomposition," *J. Graph.*, vol. 45, no. 1, pp. 65–77, 2024.

[15] A. Rosenfeld and R. Klette, "Digital geometry," *Inf. Sci.*, vol. 148, no. 1, pp. 123–127, 2002. doi: 10.1016/S0020-0255(02)00284-0.

[16] Z. Yang, S. Soltanian-Zadeh, and S. Farsiu, "BiconNet: An edge-preserved connectivity-based approach for salient object detection," *Pattern Recognit.*, vol. 121, no. 12, 2022, Art. no. 108231. doi: 10.1016/j.patcog.2021.108231.

[17] M. Kampffmeyer, N. Dong, X. Liang, Y. Zhang, and E. P. Xing, "ConnNet: A long-range relation-aware pixel-connectivity network for salient segmentation," *IEEE Trans. Image Process.*, vol. 28, no. 5, pp. 2518–2529, 2019. doi: 10.1109/TIP.2018.2886997.

[18] Y. Jia, M. Salzmann, and T. Darrell, "Factorized latent spaces with structured sparsity," in *Adv. Neur. Inf. Process. Syst. 23: 24th Annu. Conf. Neural Inf. Process. Syst. 2010*, Vancouver, BC, Canada, 2010.